Summer 1993

Light Injection from an Active Cladding to the Core of a Fiber Optic Fluorosensor

Alvin Leon Bryant
Old Dominion University

LIGHT INJECTION FROM AN ACTIVE CLADDING TO THE CORE OF A FIBER OPTIC FLUOROSENSOR

by

Alvin Leon Bryant

B.S.E.E. December 1991, Old Dominion University

A Thesis Submitted to the Faculty of
Old Dominion University in Partial Fulfillment of the
Requirements for the Degree of

MASTER OF SCIENCE

ELECTRICAL ENGINEERING

OLD DOMINION UNIVERSITY

August, 1993

Approved by:

Dr. Sacharia Albin

Dr. Ravindra P. Joshi

Dr. Vishnu K. Lakdawala

ABSTRACT

LIGHT INJECTION FROM AN ACTIVE CLADDING TO THE CORE OF A FIBER OPTIC FLUOROSENSOR

Alvin Leon Bryant

Old Dominion University

Director: Dr. Sacharia Albin

A fluorosensor works on the basis of light injection from the clad into the core of an optical fiber. The sensitivity of such a sensor depends on the efficiency of light injection. Conditions necessary for a high injection efficiency are experimentally determined. The refractive index difference between the core and the clad, n_{core}-n_{clad}, must be maximized to achieve a high injection efficiency. Since an air clad has the least refractive index, a bare core fiber will have a maximum efficiency. Standard optical fibers used for communication employ a minimum value for n_{core}-n_{clad}, in order to reduce modal dispersion and increase the usable diameter. These fibers do not have a high efficiency and hence they are not suitable for fluorosensor applications. The injection efficiency is found to increase with the fiber diameter. The experimental results are in good agreement with the theoretical models based on a weakly guiding approximation and an exact field solution.

ACKNOWLEDGEMENTS

I would like to thank Dr. Ravindra Joshi and Dr. Vishnu Lakdawala for assisting in bringing this research to a close. Thanks go to Mr. Glen Farnsworth and Mr. Mert Felts for preparing the fibers; their time and patience is well appreciated.

Many thanks go to Bhaskar Bulusu and Arnel Lavarias for their assistance in the lab. Knowing and working with them has been a pleasure. I specially thank Lin Watkins and Jim Satira for their help and expertise in the Photonics Lab.

I am deeply indebted to Dr. Claudio Egalon and Dr. Robert Rogowski for their support and many technical discussions. Their help was instrumental in this work. I would like to thank NASA Graduate Researchers Fellowship Program for the financial assistance.

I would like to thank my family for their support throughout my college years. Especially, I thank my wife, Cheryl, for her patience, encouragement and support.

Last but not least, I would like to thank Dr. Sacharia Albin for his experience guidance, and encouragement, during my time at Old Dominion University. He has been an excellent advisor as well as a good friend.

TABLE OF CONTENTS

LIST OF TABLES

LIST OF FIGURES

CHAPTER 1
INTRODUCTION

In the early 1970's, researchers investigating optical fiber communication realized that physical perturbations could modulate light guided in a fiber [1]. The availability of low loss optical fibers with the associated small size, light weight, and wide bandwidth, has led to the development of fiber optic sensors (FOS). These sensors can measure a wide variety of physical and chemical parameters such as temperature, acceleration, pressure, rotation, displacement, current, electromagnetic and nuclear radiation, pH, humidity and chemical species [2-7]. Currently, FOS are actively used in aerospace, medicine, industry, defense and environmental systems. These sensors exploit the quantum and wave nature of light. Due to the high speed at which light travels, FOS are able to respond fast to changes in the sensed parameter. In its simplest form, a FOS consists of a light source, an optical fiber and a detector. In general, depending on the role of the fiber, FOS are categorized as extrinsic or intrinsic.

1.1 Extrinsic Sensor

Extrinsic sensors use fibers strictly as waveguides to carry the information. The input fiber directs the light to a transducer element which

modulates the light beam and then couples the beam to one or more output fibers. The transducer is the element which responds to variations in the physical parameters. An excellent example of an extrinsic sensor is the pressure sensor based on the photo-elastic effect, as shown in figure 1 [2]. With the photoelastic effect, A transparent isotropic material becomes anisotropic under applied stress. This stress-induced birefringence can be related to the applied pressure. Fiber sensors using these materials are configured so that applied pressure modulates the intensity of the guided light. Here, the input and output fibers act merely as waveguides. Similar extrinsic transducer elements can be used to sense other parameters.

1.2 Intrinsic Sensor

In the intrinsic type, the optical fiber itself is the active transducer element, in addition to being a waveguide. The properties of the fiber determine the type of modulation. The microbend sensor is an example of an intrinsic sensor as shown in figure 2. The pressure applied on deformers alter the guiding condition of the fiber by causing bending losses. The reduction in signal intensity due to the applied pressure can be easily measured [8]. In addition to the intensity modulation, phase or polarization can also be altered. As noted above, common to both types are the optical sources, detectors and signal processing electronics. Since the intrinsic sensors make use of the fiber as the transducer, they can be configured as distributed sensors to yield sensing information from different points along the fiber.

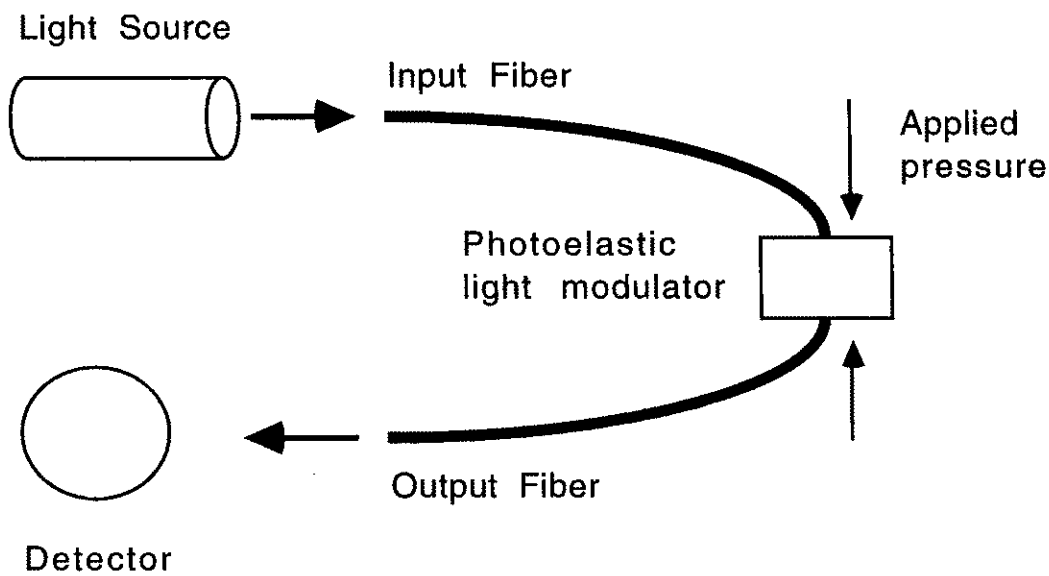

Figure 1. An extrinsic sensor based on the photoelastic effect.

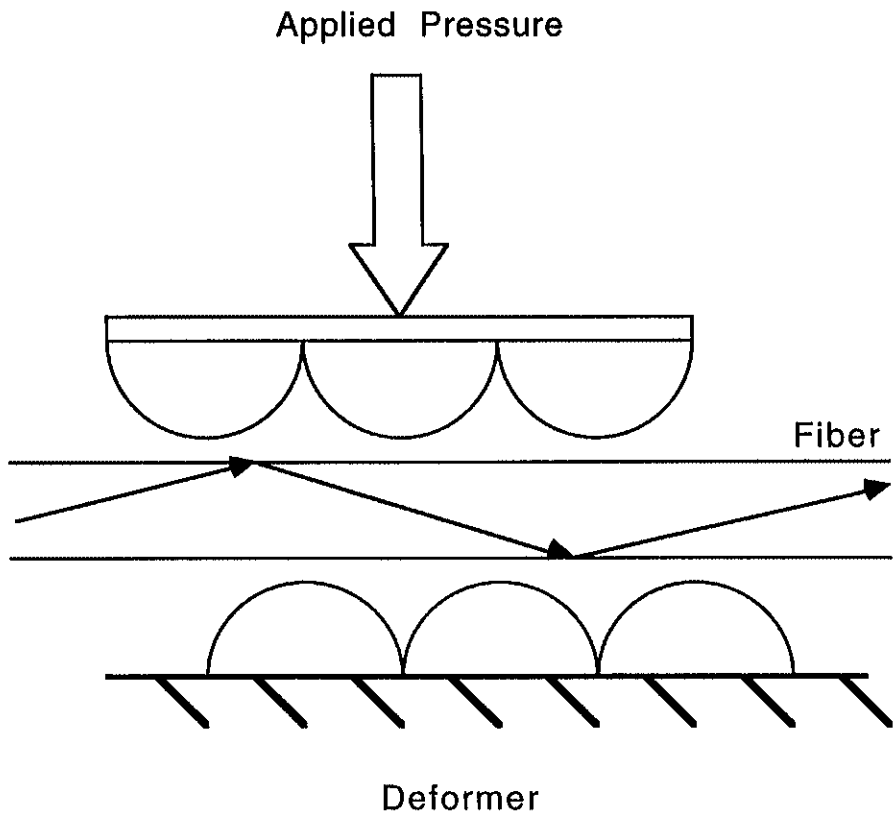

Figure 2. Representation of an intrinsic microbend sensor.

1.4 Fluorosensor

A new form of an intrinsic sensor which is well suited to sensing chemical and biological species is the fluorosensor. The name fluorosensor has been coined to describe a sensor that employs an optical fiber with a fluorescent core or clad. A fluorescent core can be excited by the bound modes of light propagating in the fiber or by external radiation penetrating the clad. For active cladding fluorosensors, as represented in figure 3, the excitation can be achieved by the evanescent field of the guided wave in the core or by external sources directly exciting the cladding sources. The spectral properties of the fluorescence will be affected by external parameters. For example, Lieberman et. al., have developed an oxygen sensor based on the fluorescence quenching of 9,10-diphenylanthracene incorporated into the cladding [9]. Excitation of the fluorescent material was achieved by externally pumping the fluorescent region. A thirty percent reduction in fluorescence intensity was observed when the ambient surrounding the clad was changed from nitrogen to oxygen. Similarly, a radiation sensor is under development in our laboratory using a stimulated electronic transition (SET) material in the cladding [10]. Here, external radiation excites the SET material and the fluorescence emitted is coupled to the core and guided to a detector.

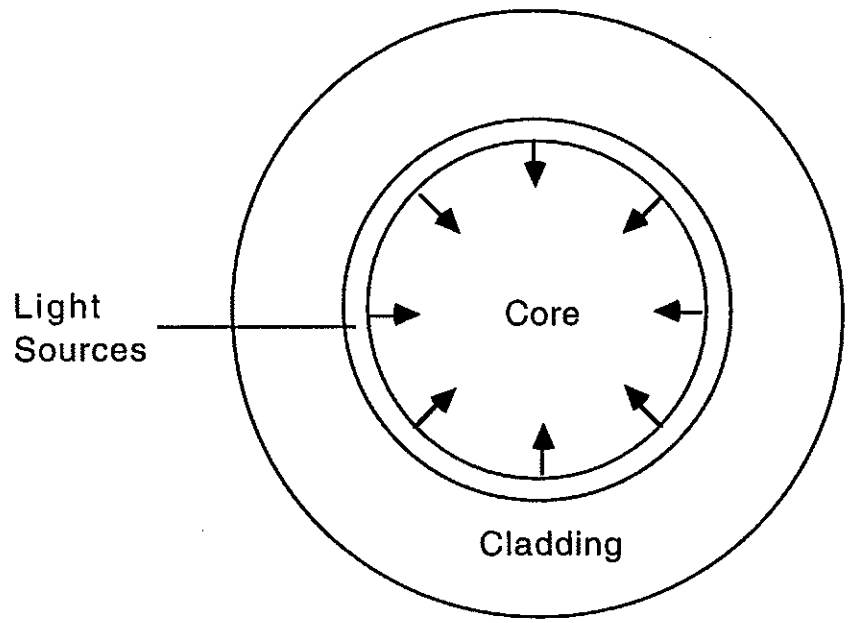

Figure 3. Representation of an active cladding fluorosensor.

1.5 Goals of this Study

Optimum performance of the cladding fluorosensors described above, depends on the injection of light from the cladding to the core. There have been a few theoretical studies on this coupling efficiency; however, no systematic experimental work has been reported so far. In this work, the main topic of investigation is the effect of refractive index difference between the core and the cladding on the coupling of cladding fluorescence into the fiber core. The numerical aperture (NA) of the fiber depends on the refractive index difference between the core and the clad. In the case of the fluorosensor, the NA is investigated at the sensing region rather than the ends of the fiber. In addition, the effect of variation of the core diameter on the coupling is investigated. For a given NA and a fixed wavelength, the V-number depends on the core diameter . Hence this part of the study is to determine the effect of V-number on the injection of light from the clad. Finally, a comparison will be made between the existing theory and our experimental results.

CHAPTER 2

THEORY OF LIGHT INJECTION FROM CLAD TO CORE

Although some details and principles of evanescent wave fluorosensors have been established, a complete and quantitative theory is not currently available [11-14]. The system to be studied, a bare fiber core coated with a thin film of fluorescent material, involves two processes. The first process is excitation of the fluorescent sources. This can be achieved by the interaction between the fluorescent molecules and the evanescent component of a wave travelling within the fiber. External excitation such as chemiluminescence and laser induced fluorescence can also be used. The second process is injection of the fluorescence into the core. This process is key to the operation of a fluorosensor. Therefore, our primary aim is how to best launch cladding fluorescence into the fiber core. In this chapter we discuss the theoretical models governing active cladding fluorosensors. We first examine the interaction of light at a plane boundary of two dielectric medium. The fundamentals of evanescent waves at planar interfaces are then extended to cylindrical geometries. Next, the principles of the weakly guiding approximation, a model so commonly used for communication fiber, is discussed. This chapter concludes with a discussion on a theoretical model for the power injection efficiency of an active cladding fluorosensor based on exact field solutions.

2.1 Planar Waveguide

When an optical high-index dielectric is sandwiched between a low-index substrate and a low-index top layer, a planar slab waveguide is formed. For simplicity, we shall consider the case of a symmetric structure where the indices of the substrate and top layer are identical, denoted as n_2. These low-index surrounding layers are termed the cladding regions of the waveguide. Let the refractive index of the guiding layer or core be n_1, where $n_1 > n_2$ is a necessary condition for guiding. figure 4 shows that light rays incident at the interface of two dielectric medium will be totally internally reflected when the ray angle exceeds the critical angle, θ_c. The critical angle is given by Snell's Law:

$$\theta_c = \sin^{-1}\left(\frac{n_2}{n_1}\right) \qquad (2.1).$$

A more detailed examination of the rays interaction at the interface reveals that for distances very close to the interface there is a nonpropagating or evanescent wave present in the cladding region. figure 5 illustrates the trajectory of the evanescent wave in the interface region. In the cladding, the amplitude of the evanescent field is given by [11, 15]:

$$E = E_o \exp\left[j\left(\omega t - \frac{2\pi n_1}{\lambda} z\sin\theta\right) - \frac{y}{\delta_p}\right] \qquad (2.2),$$

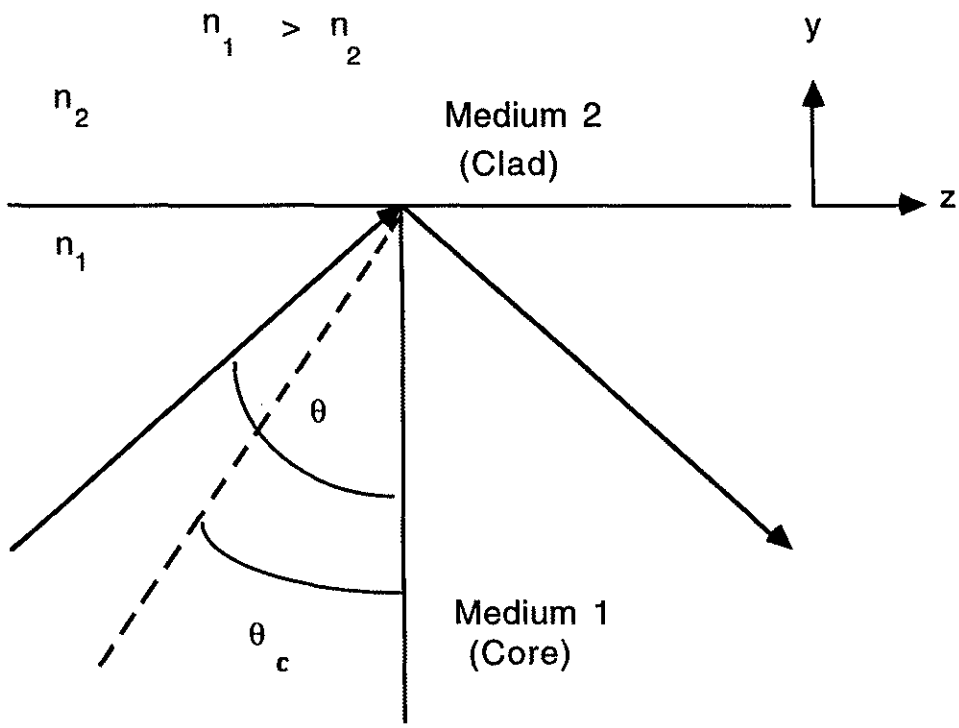

Figure 4. Light rays at a dielectric interface. Rays incident at angles exceeding the critical angle are totally internally reflected.

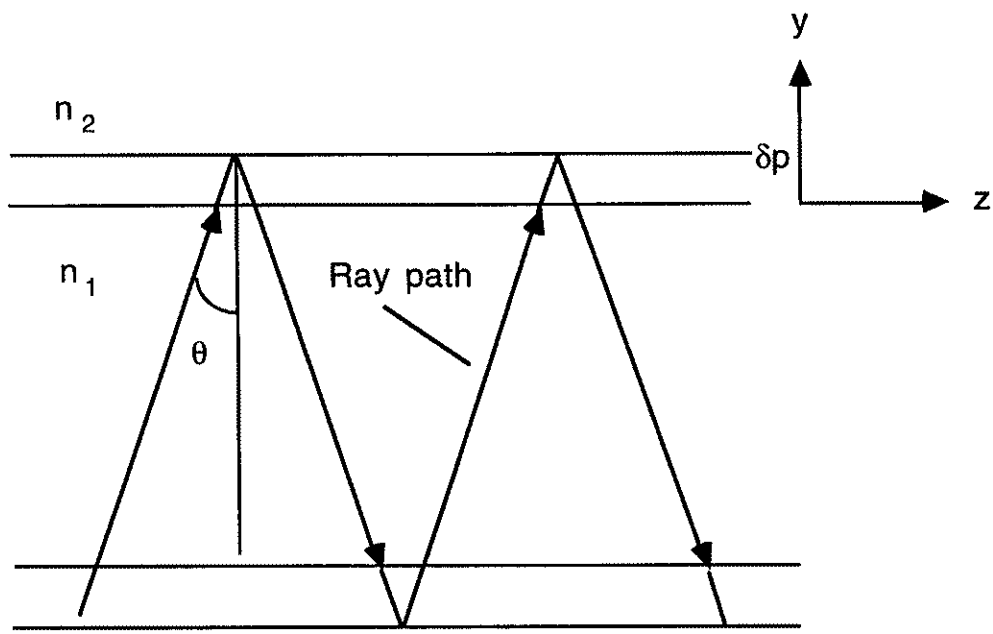

Figure 5. Light rays penetrating into the clad region.

where $$\delta p = \frac{\lambda}{2\pi\left[n_1^2 \sin\theta - n_2^2\right]^{1/2}} \quad , \qquad (2.3)$$

the penetration depth, is the distance at which the amplitude falls to 1/e of its value at the interface. Equation (2.2) states that the amplitude of the evanescent wave decays exponentially away from the interface and its direction of propagation is parallel to the waveguide axis (z-direction).

The evanescent field can interact with molecules in the cladding region near the interface, where it can be absorbed and used to excite fluorescent sources, provided the wavelength is appropriate. Conversely, the principle of reciprocity gives rise to a finite probability that the inverse process can occur, ie. the emission of evanescent waves by excited molecules in the cladding. If the cladding has excited molecules emitting light near the interface, we should be able to detect radiation propagating at angles exceeding the critical angle (figure 6). Such high angle emission corresponds to the evanescent wave of the guided modes.

2.2 Cylindrical Waveguide

Although a rigorous treatment of cylindrical waveguides involves Bessel functions and finding the eigenvalues of all guided modes of the waveguide, simpler approximations may be valid under certain conditions. When the diameter of a cylindrical waveguide is large compared to the wavelength of light, the individual reflections of the guided waves at the core-cladding interface can be described to a good approximation

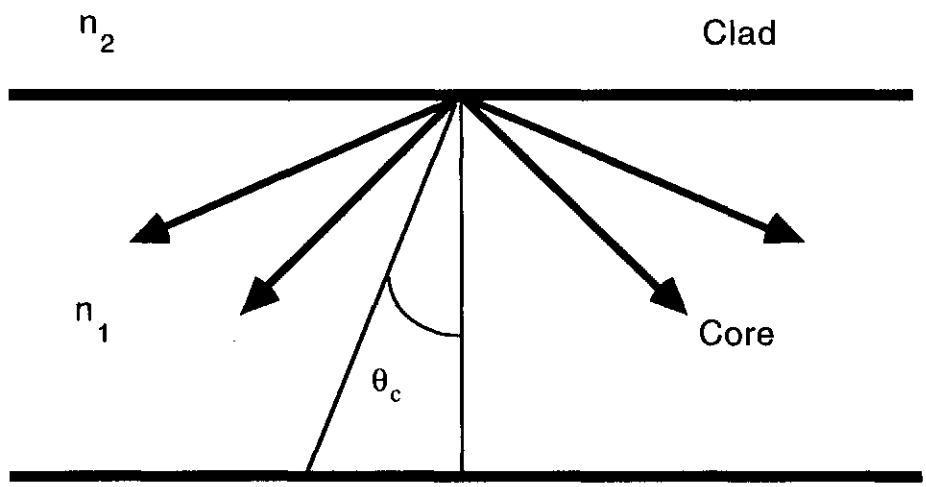

Figure 6. Light injection into the core due to clad sources.

as reflections from a planar interface [11]. Thus, a cylindrical fiber sensor can be characterized by summing the contributions from individual rays, each ray is analyzed as though it interacts with a plane. Using the results from the planar geometry as a building block, Love et al. have performed calculations to model the collection of cladding fluorescence from a fluorosensor [11]. Each ray coupled into the fiber core is considered an independent producer of fluorescence; the total signal is obtained by adding the signals generated by each ray. For fluorescent molecules near the interface, they derived an expression for the total fluorescent signal available at one end of the fiber. The total signal intensity, S_{TOT}, is reported to be [11]:

$$S_{TOT} \alpha I_o L a \lambda \frac{1}{\left(n_{core}^2 - n_{clad}^2\right)^2} \quad , \qquad (2.4)$$

where I_o is the optical source radiance, a is the core radius, L is the length of the fluorescent region, and n_1 and n_2 are the core and cladding refractive indices respectively. Throughout this thesis, we shall interchangeably use n_{core} and n_1 to denote the index of refraction of the core and similarity, n_2 and n_{clad} to denote the refractive index of the cladding region. Equation (2.4) predicts that the fluorescent signal strength will decrease with increases in index differences, $n_{core} - n_{clad}$. figure 7 shows the predicted behavior of fluorescent signal versus NA, which is defined as $\sqrt{\left(n_1^2 - n_2^2\right)}$. The dashed curves predict the behavior for a thin-film of sources and the solid curve predicts the behavior for a bulk distribution of sources.

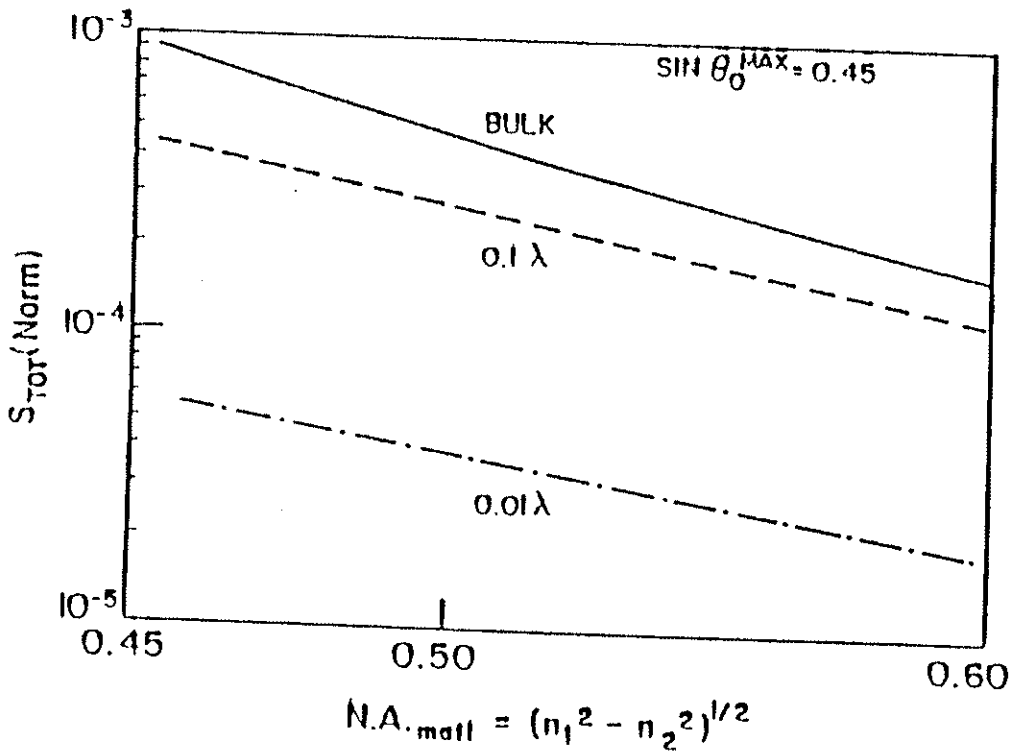

Figure 7. Variation of total fluorescent signal, S_{TOT}, with NA (From reference 11).

2.3 Weakly Guiding Approximation

The injection of light from cladding sources has also been theoretically treated by Marcuse [12]. In his approach, the weakly guiding approximation for guided modes was used to formulate an expression for the collection efficiency of active cladding fluorosensors. The weakly guiding approximation greatly simplifies the vectorial analysis of guided modes in a cylindrical waveguide by allowing a scalar treatment of the electric and magnetic fields of guided waves. The criterion for this approximation is the core-cladding index difference, $n_{core} - n_{clad}$, be small. The weakly-guiding approximation is based on the observation that for small $n_{core} - n_{clad}$ values, the critical angle, θ_c, at the interface is very large. Hence, guided modes inside the core are almost parallel to the axis of propagation. Since the total field inside the waveguide may be considered by summing of similar waves, the combined electric and magnetic vectors must be almost exactly orthogonal to each other, and to the fiber axis. Thus, the two dimensional spatial dependence of the fields is suppressed, allowing for scalar approximations.

The term collection efficiency or power efficiency is defined to be the ratio of light collected in the fiber core relative to the total amount of light radiated by the sources in the absence of the fiber core, P_{core} / P_{clad}. The expression for the collection efficiency from a thin-film of sources is reported by Marcuse as [12]:

$$\frac{P_{core}}{P_{clad}} = \frac{1}{2\, n_{core}^2\, k^2 V^2 a^2} \sum_n \frac{(\gamma a)^2\, J_v^2(Ka)}{|J_{v-1}(Ka)\, J_{v+1}(Ka)|} \qquad (2.5)$$

where $$V = \frac{2\pi a}{\lambda}\sqrt{n_{core}^2 - n_{clad}^2} \qquad (2.6)$$

is the modal volume, $\gamma = \sqrt{\beta^2 - n_{clad}^2 k^2}$ is the radial decay parameter, $k = 2\pi/\lambda$ is the wavenumber, $K = \sqrt{n^2 \quad k^2 - \beta^2}$ is the radial propagation constant, β is the axial propagation constant, and $J\upsilon$ is the Bessel function of order υ.

Within the weakly-guiding approximation the solution of the eigenvalue equation depends only on V. This means the sum terms in equation (2.5) are universal functions of V [12]. Therefore, one can not perceive the character of the collection efficiency from equation (2.5) by inspection. If the emission wavelength and the core radius are assumed fixed, an increase in V-number corresponds to an increase in the core-cladding index difference. Figure 8 shows a plot based on equation (2.5). We see the collection efficiency grows with V in a parabolic manner. Relating V to the index difference, $n_{core} - n_{clad}$, we see that the fluorescence collected by the core as guided modes is directly proportional to $n_{core} - n_{clad}$. This result does not agree with the theoretical predictions previously discussed in section 2.2.

2.4 Exact Field Solution

The results of light injection into the fiber core presented above have made use of the weakly guiding approximation. This approximation simplifies the analysis of collection efficiency, but can not accurately predict the behavior of light coupled in a fiber with arbitrary differences

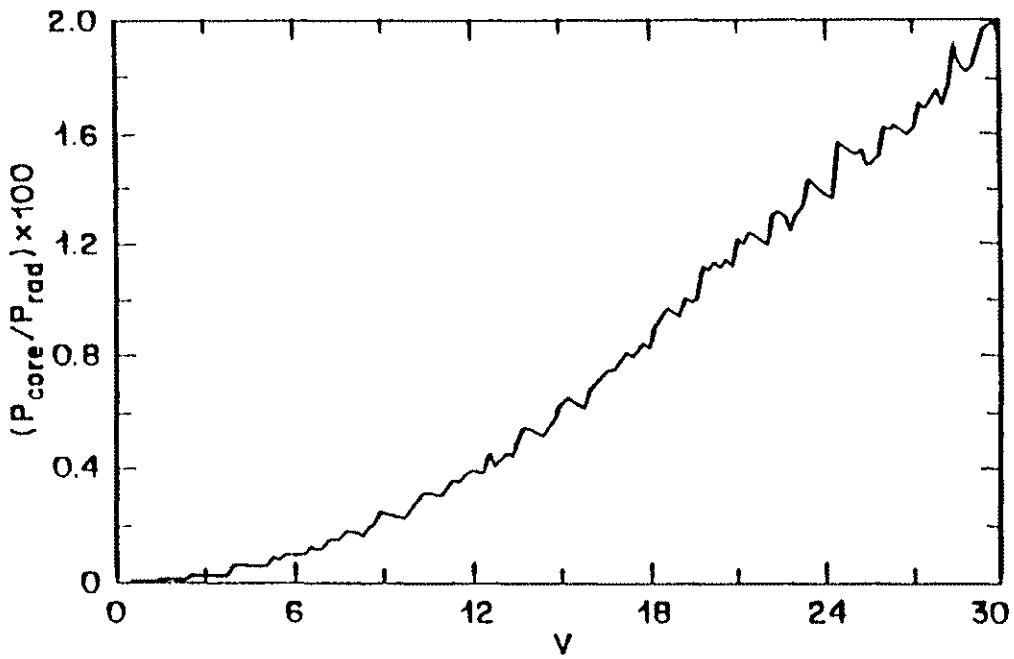

Figure 8. Collection efficiency versus V-number (From reference 12).

in refractive indices. Egalon and Rogowski have used the exact field solution to develop a expression for the power efficiency, P_{eff}, and analyzed its behavior as a function of $n_{core} - n_{clad}$ as well as a number of other parameters [13]. The power efficiency is defined in the same manner as the collection efficiency in section 2.3. The expression governing the power efficiency for a fiber coated with a thin-film of fluorescent sources at the dielectric interface is given as [13,14]:

$$P_{eff} = \frac{P_{core}}{P_{clad}} = \frac{\sqrt{\epsilon_o/\mu_o}}{8a\delta L n_{clad} k^2} \sum_{\nu,\mu} \frac{1}{P_{\nu,\mu}} \int_{V_{source}} |e_{\nu,\mu}|^2 dV \qquad (2.7),$$

where L is the length of the thin-film, k is the wavenumber of the fluorescent light, δ is the film thickness, and $P_{\nu,\mu}$ is a normalization constant ϵ_o and μ_o is the permittivty and permeability of free space and $|e_{\nu,\mu}|^2$ is the modal electric field modulus. For the exact solution, the integral term in equation (2.7) has to be computed for each type of mode separately: transverse electric (TE), transverse magnetic (TM), and hybrid modes (EH and HE). The expressions for integrals of these modes are too involved and will not be given here; instead the interested reader is directed to [14] for more details. A plot of the power efficiency of a thin-film of sources based on the above equation is shown in figure 9. In this figure the power efficiency is plotted versus n_{core}. In the calculations, the cladding index was held fixed at, $n_{clad} = 1.0$, while the core index is varied. In this case, increases in the core index also increases in the index difference, $n_{core} - n_{clad}$.

Figure 9 indicates the power efficiency increases almost linearly with n_{core} and hence, $n_{core} - n_{clad}$. This result is in agreement with those obtained using the weakly guiding model and in direct contradiction with that reported previously in section 2.2. To validate these theories, no experimental work has been reported so far. This study is the first attempt to verify experimentally the theoretical results discussed above.

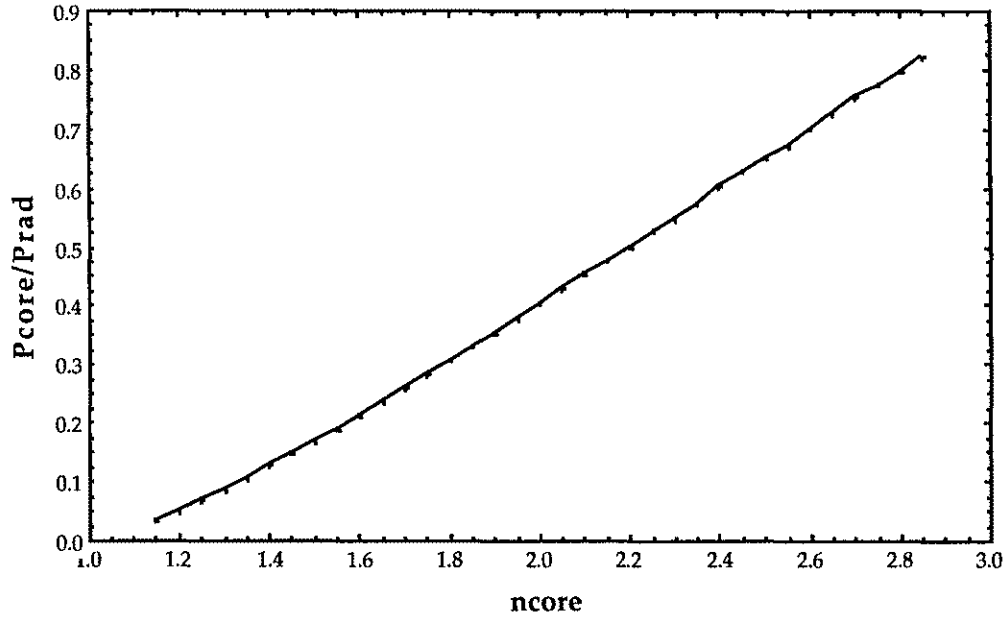

Figure 9. Power efficiency of a thin-film of sources versus n_{core} using the exact field solution. (From reference 13).

CHAPTER 3

EXPERIMENTAL METHODS

3.1 Fiber Preparation

Fibers of various diameters were drawn from a 6 mm diameter quartz rod (refractive index 1.459) using glass blowing techniques. Attenuation curves show high losses for wavelengths above 2 μm. The drawn fibers were uniform in diameter for short lengths which were sufficient for our experiments. The fibers were cleaved to a length of 18 cm. Each fiber was examined under a Leitz microscope. These fibers were coated with a luminescent thin-film about 2 cm long region at one end of the fiber using the procedure given below.

3.2 Fluorescent matrix

The fluorescent material consists of Y_2O_3:Eu^{3+} which is a luminescent powder available from GTE Sylvania (type #1134). It was incorporated into a polymer precursor PDMS (McGhan NuSil R2615) which is a viscous liquid in its basic form and can be cured by using an appropriate catalyst. Xylene was added to this mixture to thin the liquid. The coating consisted of 0.5g of Y_2O_3:Eu^{3+}, 1g of PDMS base, 0.15g of PDMS cure, and 0.5g of xylene. Each fiber was dip-coated for appropriate thickness and cured in an oven at 200 ^{o}C for ten minutes. For optical measurements, the fibers were placed in a cell which is described below.

3.3 The fiber cell

The schematic diagram of the fiber cell is shown in figure 10. The cell was constructed from a transparent plastic cylindrical tube (refractive index 1.477). A small section was cut away along the axis and a hole formed so that the cell could be filled and emptied with liquid solutions. The inside and outside surfaces of the cell were painted flat black except for a rectangular window region which acted as an aperture. Two annular rubber discs were inserted into the ends of the plastic tube and two rubber membranes with a pinhole covered the discs. The fiber was held in place by the membrane which sealed the cell. The coated region of the fiber was located between the two discs in the cell. The volume between the fiber and the inner wall of the cell can be thought of as a cladding. This volume was filled with air or liquids of different refractive indices.

3.4 Refractive index variation of clad

There are many commercially available liquids which be could be used to fill the volume of the cell. To achieve better control of the refractive indices of the liquids used in this work, we used aqueous solutions of sucrose. Water has a refractive index of 1.333 at room temperature. By adding sugar to water, refractive indices can be varied from 1.333 to 1.500 [16]. Figure 11 shows the variation of refractive index versus percentage of sugar by mass. Tables 1 and 2 list the refractive indices of the solutions, fibers, PDMS, and fiber cell.

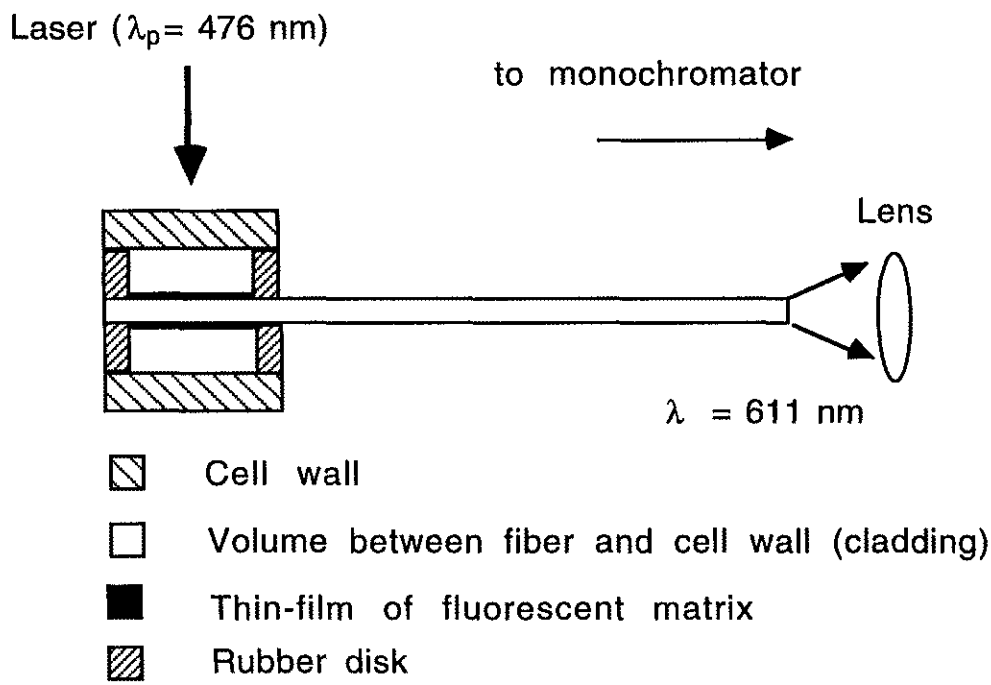

Figure 10. Schematic of the fiber cell.

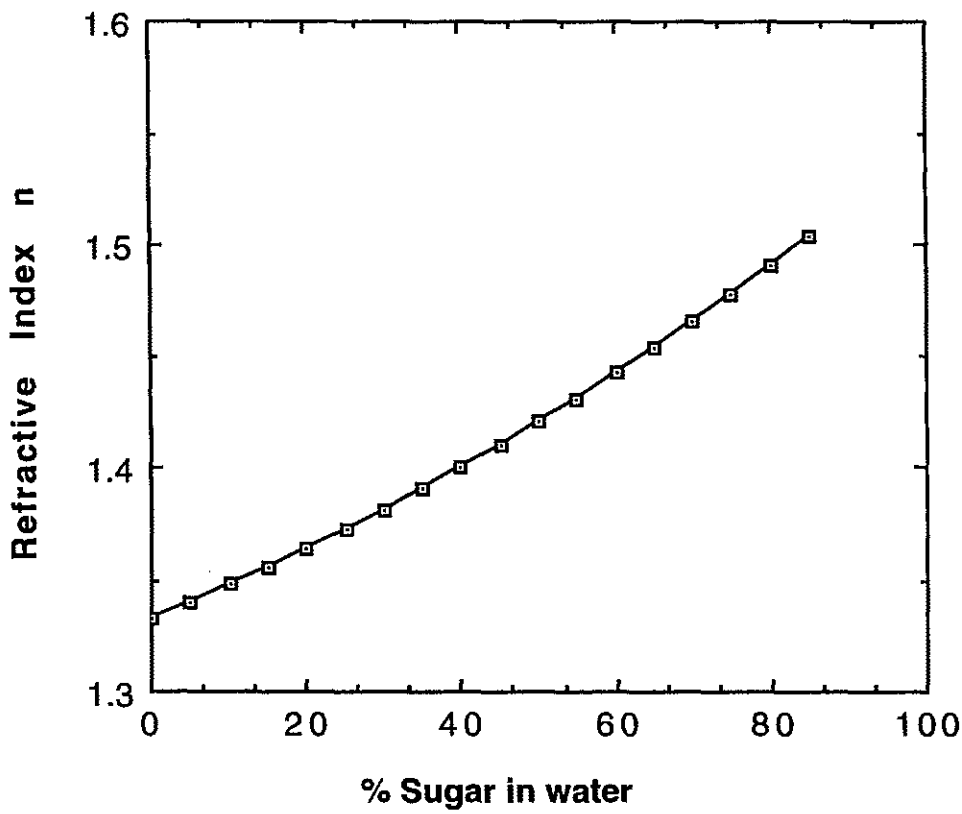

Figure 11. Refractive index change versus sugar concentration.

Table 1. Refractive indices for cladding solutions.

Cladding	Refractive index (n_{core})	$n_{core} - n_{clad}$
air	1.000	0.459
water	1.333	0.126
solution #1	1.347	0.112
solution #2	1.358	0.101
solution #3	1.369	0.090
solution #4	1.378	0.081
solution #5	1.386	0.073
solution #6	1.394	0.065

Table 2. Refractive indices of materials.

Material	Refractive index
Cell	1.477
PDMS	1.406
Fibers	1.459

The refractive indices of the solutions and the cell were obtained using an Abbe's refractometer whereas the values for the remaining materials were obtained from their respective manufacturers.

3.5 Spectroscopic setup

The experimental setup used to measure the spectral properties of the fluorescence from the fibers is shown in figure 12. The system consists of a continuous wave argon ion laser (Spectra Physics Stabalite 2011) , a 0.64 meter monochromator (Instruments SA HR 640) fitted with a Spectra Link data acquisition interface module, and a water-cooled photomultiplier tube (PMT) (Hamamatsu 928s). The laser gives five different lines ranging from 454.5 to 514.5 nm. The 476.5 line was chosen because it corresponded to a local absorption peak of Y_2O_3:Eu^{3+} [17]. Laser power was set at 800 mW. The monochromator has a spectral range of 200 nm to 3 μm with interchangeable gratings. The resolution of the monochromator is 0.1 Angstrom. The spectral response of the PMT ranges from 200 to 850 nm. The wavelength setting of the monochromator and the PMT bias voltage were controlled by computer. The monochromator was scanned at 0.1 nm steps over the region corresponding to the emission wavelengths. The PMT signal was integrated for one second to obtain an average intensity value at each wavelength.

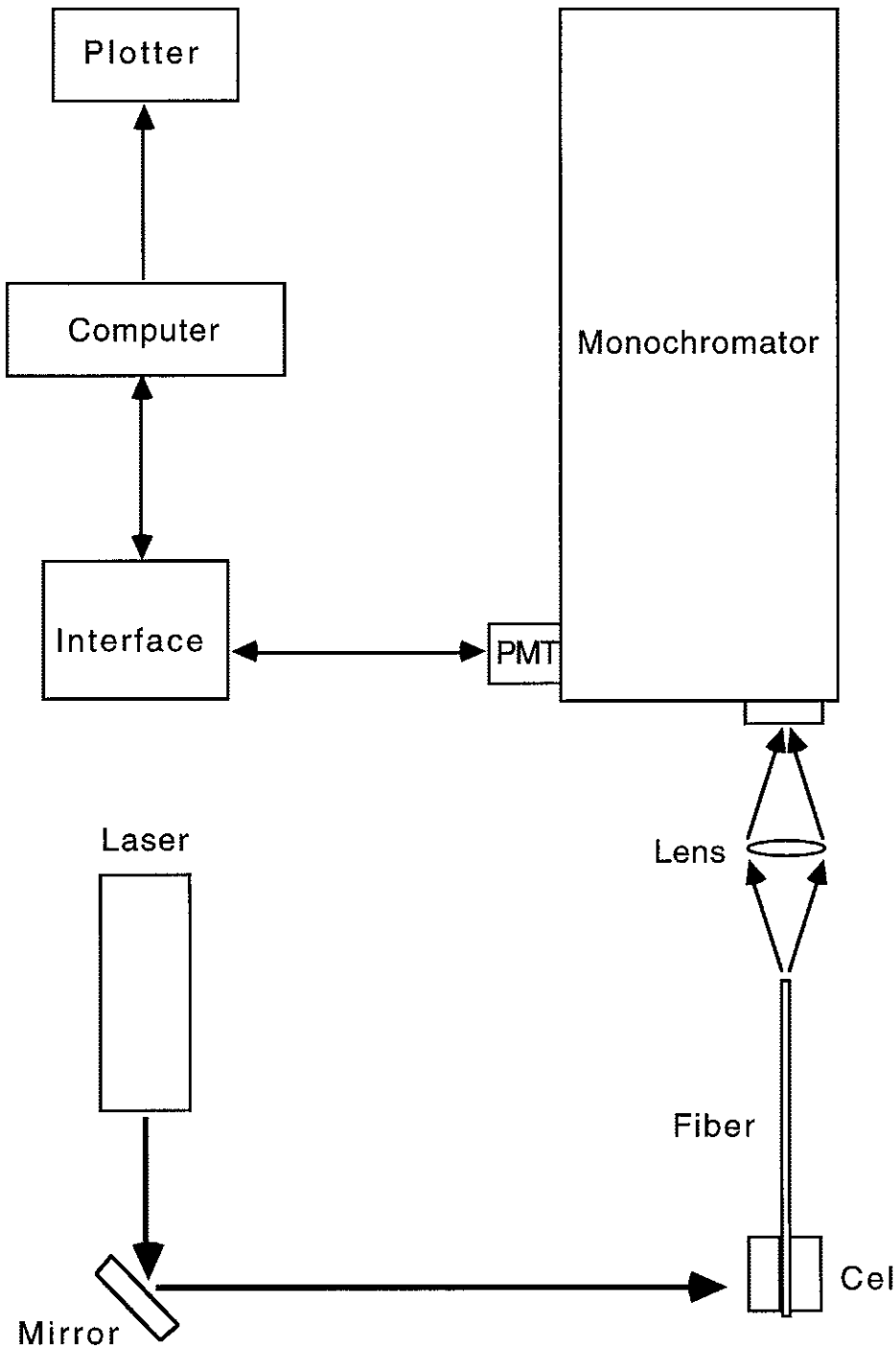

Figure 12. Spectroscopic setup used for obtaining fluorescence spectra.

CHAPTER 4

RESULTS AND DISCUSSION

With the experimental set up described in chapter 3, the fluorescent sources in the cladding region of the fibers were excited by the laser at normal incidence. Some of the radiation emitted by $Y_2O_3:Eu^{3+}$ was trapped inside the fiber as bound modes. This radiation propagated to the distal end of the fiber where it was detected. For each fiber, the emission spectrum was recorded for air and sucrose solutions in the cell surrounding the $Y_2O_3:Eu^{3+}$ sources. The peak emission intensity is proportional to the amount of radiation coupled into the core as bound modes. To determine the effect of variation in refractive index between core and clad, the intensity values were plotted for each of the corresponding core-clad refractive index difference (n_{core}-n_{clad}). To compare the absolute coupling efficiency of the fibers with different diameters, all the curves were plotted on the same graph. Then these curves were normalized to compare incremental changes.

4.1 Spectrum of $Y_2O_3:Eu^{3+}$

A typical spectral output of a fiber, due to the emission of $Y_2O_3:Eu^{3+}$ is shown in figure 13. The spectrum is characterized by a strong emission peak at 611 nm with a corresponding narrow linewidth

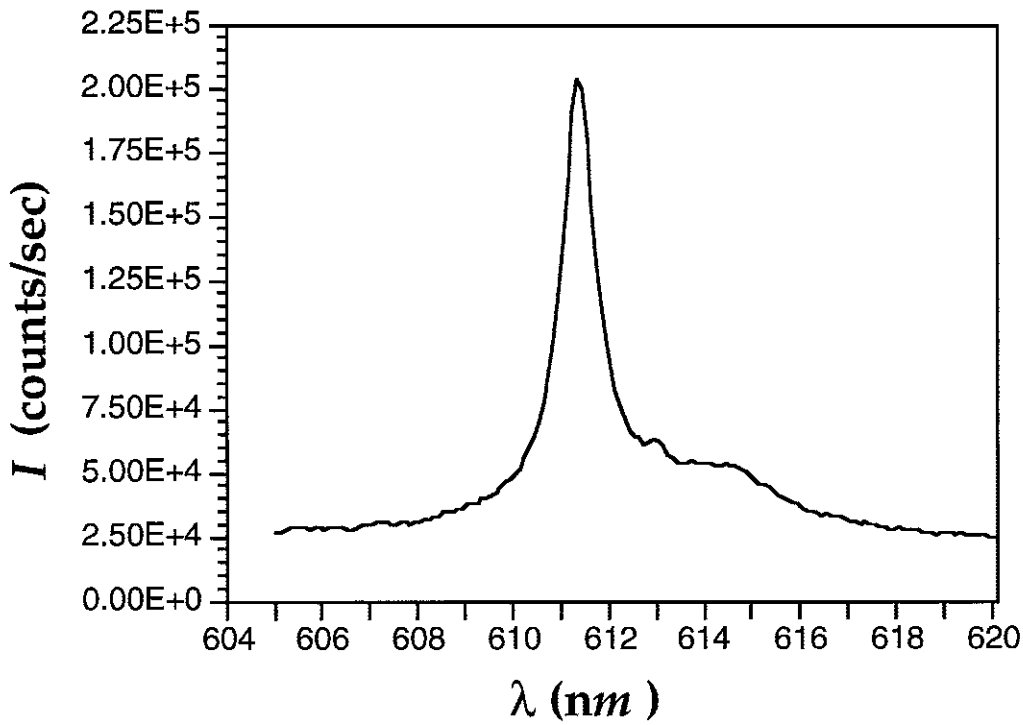

Figure 13. Spectrum of Europium doped Yttrium Oxide, $Y_2O_3:Eu^{3+}$.

(FWHM) of 9 Angstroms at room temperature [17,18]. One reason for choosing this material is its distinctive emission spectrum is readily detectable. In addition, europium doped yttrium oxide has good thermal properties. $Y_2O_3:Eu^{3+}$ has a melting point of 2410 ^oC[18]. Its emission intensity increases with temperature up to 650 ^oC and does not decrease back to room temperature level until 850 ^oC[17]. Thus, europium doped yttrium oxide is potentially a good material for high temperature sensing applications.

4.2 Intensity versus n_{core}-n_{clad}

Figure 14 shows the variation of intensity with refractive index difference, n_{core}-n_{clad}, for a fiber of 420 μm diameter . The refractive index of the cladding, n_{clad}, was varied from 1.0 to 1.394. The gap in data points is due to the unavailability of suitable cladding solutions between 1.0 - 1.333. It is clearly seen that the maximum cladding fluorescence was collected when the refractive index difference was the highest. The highest difference corresponded to an air cladding, n_{clad} = 1.0. The intensity was normalized with respect to the highest intensity (air cladding). The maximum normalized intensity, I_{nor} = 1, occurs at n_{core}-n_{clad} = 0.459, for air. Notice that the normalized intensity does increase with the difference in refractive index however, we must point out that as the cladding refractive index changes, the amount of laser power that reaches the fluorescent sources at the fiber surface also changes due to Fresnel reflection (see figure 15.).

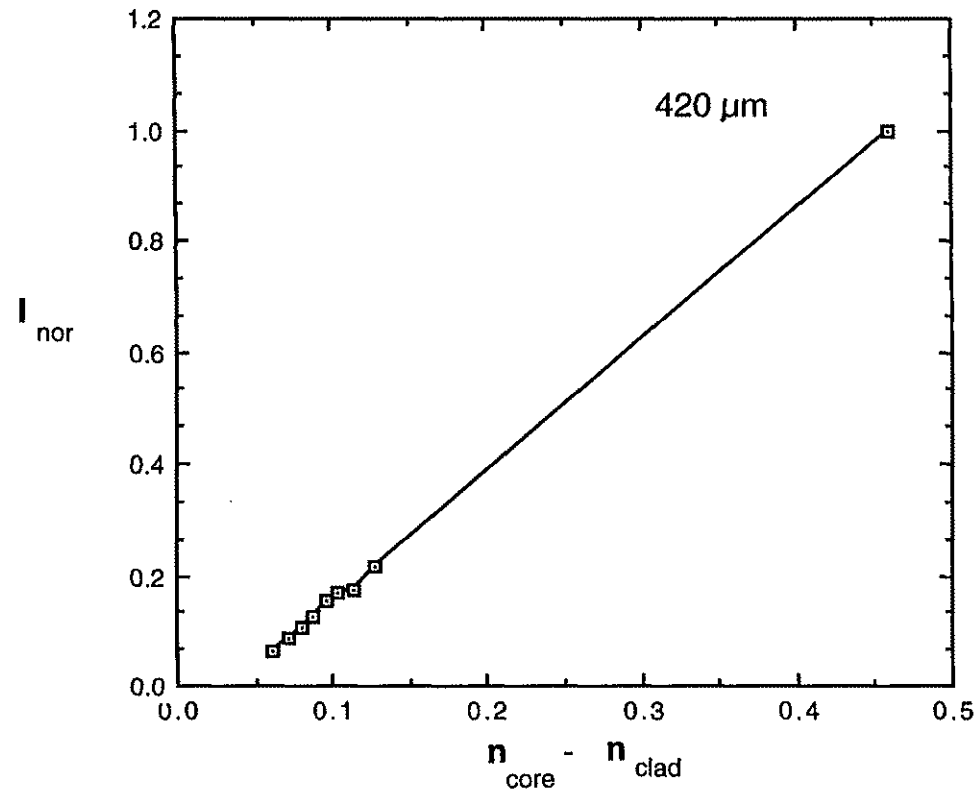

Figure 14. I_{nor} versus $n_{core} - n_{clad}$ for a 420 µm fiber.

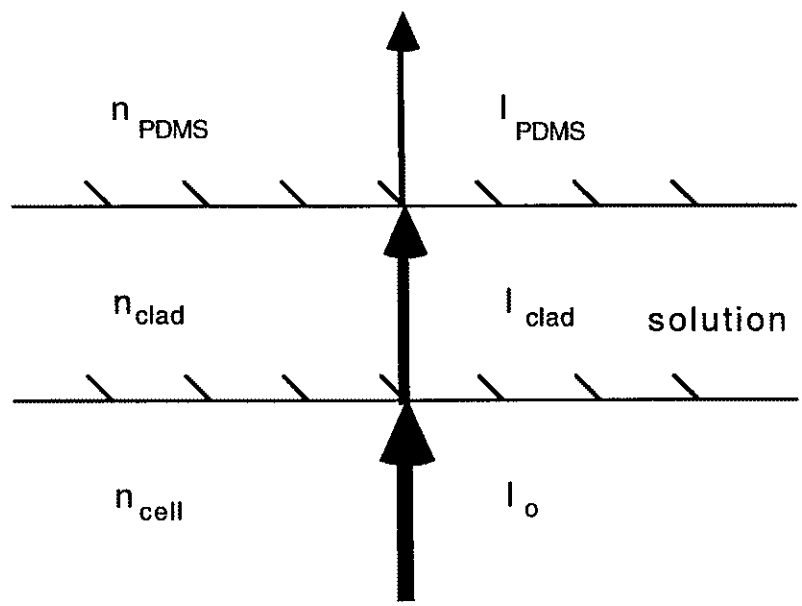

$$I_{clad} = \frac{4 n_{cell}\, n_{clad}}{(n_{cell} + n_{clad})^2} I_o \qquad I_{PDMS} = \frac{4\, n_{PDMS}\, n_{clad}}{(n_{PDMS} + n_{clad})^2} I_{clad}$$

Figure 15. Light transmission across three dielectric layers.

This occurs, because the transmission of light across the interface of two dielectric media is a function of the refractive indices of the two media; for normal incidence, the transmission coefficient is given by [19]:

$$T=\frac{4n_1n_2}{(n_1+n_2)^2} \qquad (4.1)$$

where n_1 and n_2 are the indices of refraction of media 1 and 2 respectively. Because of this effect, corrections were needed for the data points of figure 14. In our case, before reaching the fluorescent sources, the laser light has to pass through the air (n=1.0), the plastic tube (n_{cell}=1.477), the cladding surrounding the rod ($1.0 < n_{clad} < 1.394$) and finally, the fluorescent sources incorporated into the PDMS (n_{pdms} = 1.406). As the refractive index of the cladding is changes, the transmission changes, as illustrated in figure 15. Because of the additional layers of dielectric interfaces , the effective transmission coefficient of the exciting radiation just after the PDMS/cladding interface becomes [19,20.]:

$$T_{eff}=\frac{I_t}{I_o}=\frac{16n_{cell}n_{PDMS}n_{clad}^2}{(n_{cell}+n_{clad})^2(n_{PDMS}+n_{clad})^2} \qquad (4.2)$$

By analyzing equation (4.2) and the calculated T_{eff} shown in figure 16, we find that T_{eff} increases with n_{clad} and hence, it decreases with the increase in index difference, n_{core}-n_{clad}, in the interval $1.0 < n_{clad} < 1.394$, table 1 shows the values used in this work. So, as n_{clad} decreases (n_{core}-n_{clad} increases) the intensity of the exciting radiation reaching the

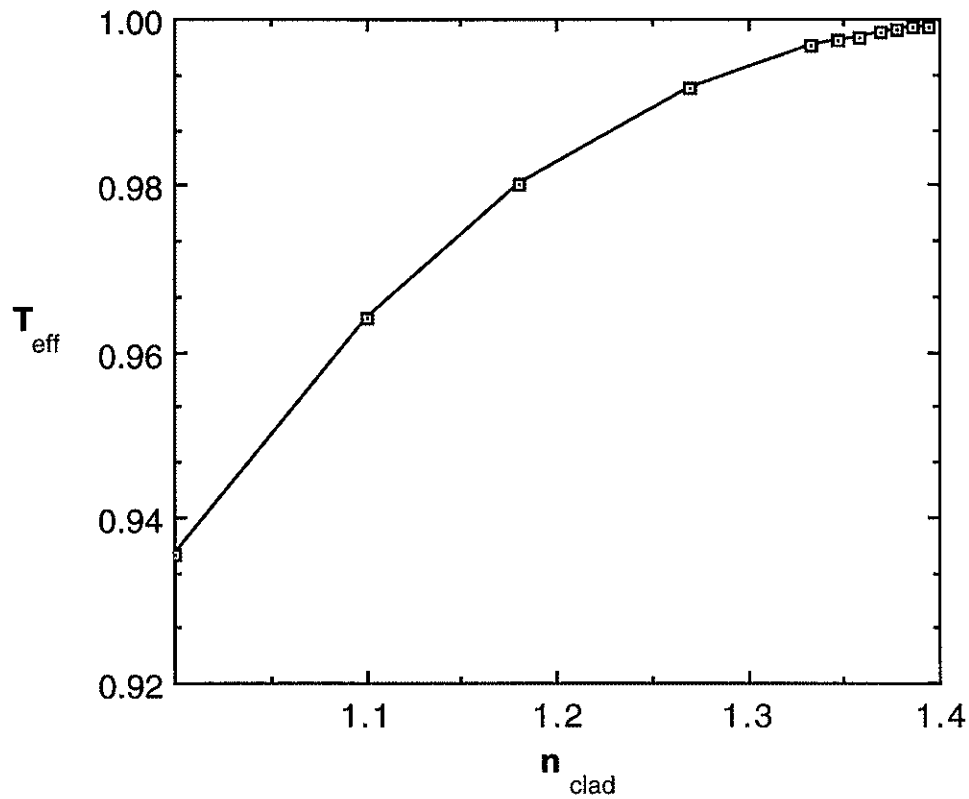

Figure 16. Effective transmission, T_{eff}, versus n_{clad}.

fluorescent sources decreases. Therefore,we should expect the corrected normalized intensity, I_{corr}, to increase slightly faster with n_{core}-n_{clad} than the uncorrected I_{nor}, shown in figure 14. Figures 17 and 18 shows the behavior of I_{corr}, which is given by the ratio I_{nor}/T_{eff}.

4.3 Diameter effect

Three intensity vs n_{core}-n_{clad} curves are shown in figure 19. These curves are not normalized, therefore the intensity, I_{eff}, is defined as I/T_{eff}, where I is measured in counts/sec. We have plotted actual intensity values to see the effect of modal volume on the light collection for the different diameter fibers. As given in equation (2.6) the modal volume is given by:

$$V = \frac{2\pi a}{\lambda}\sqrt{n_{core}^2 - n_{clad}^2} \qquad (4.3)$$

where a is the core radius and λ is the wavelength of interest. As one can see from equation (4.3), the V-number is directly proportional to the diameter. One would expect, the amount of light trapped in the fiber as bound modes to increase as the number of available modes increase. This is indeed what figure 19 indicates.

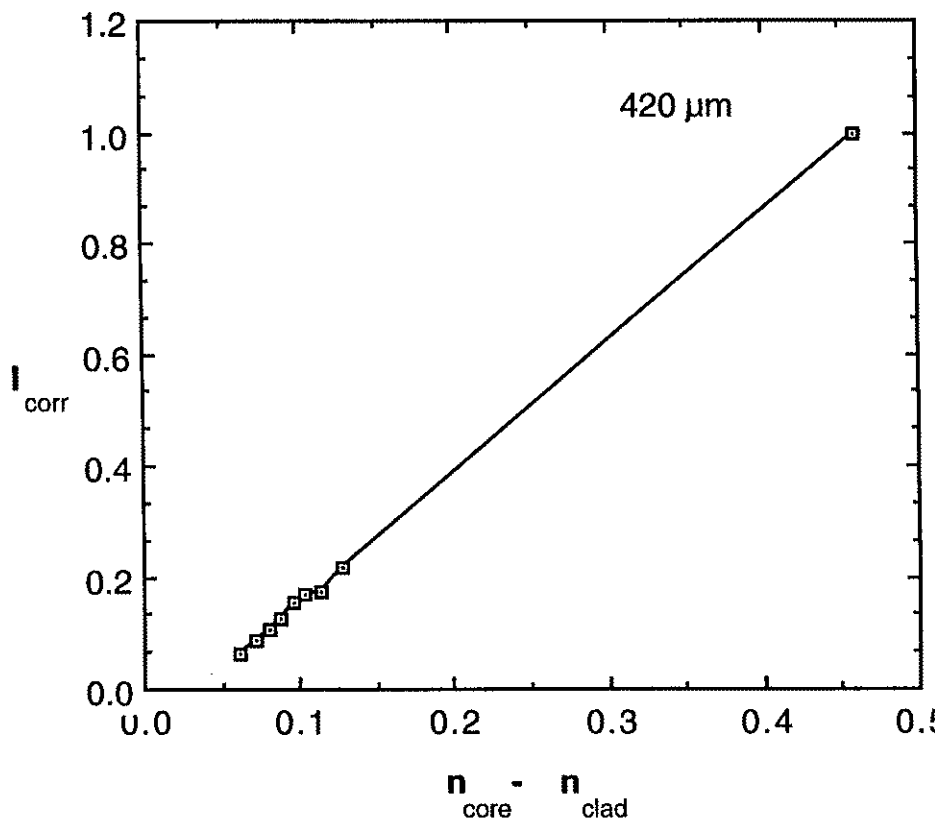

Figure 17. I_{corr} versus $n_{core} - n_{clad}$ for a 420 µm diameter fiber.

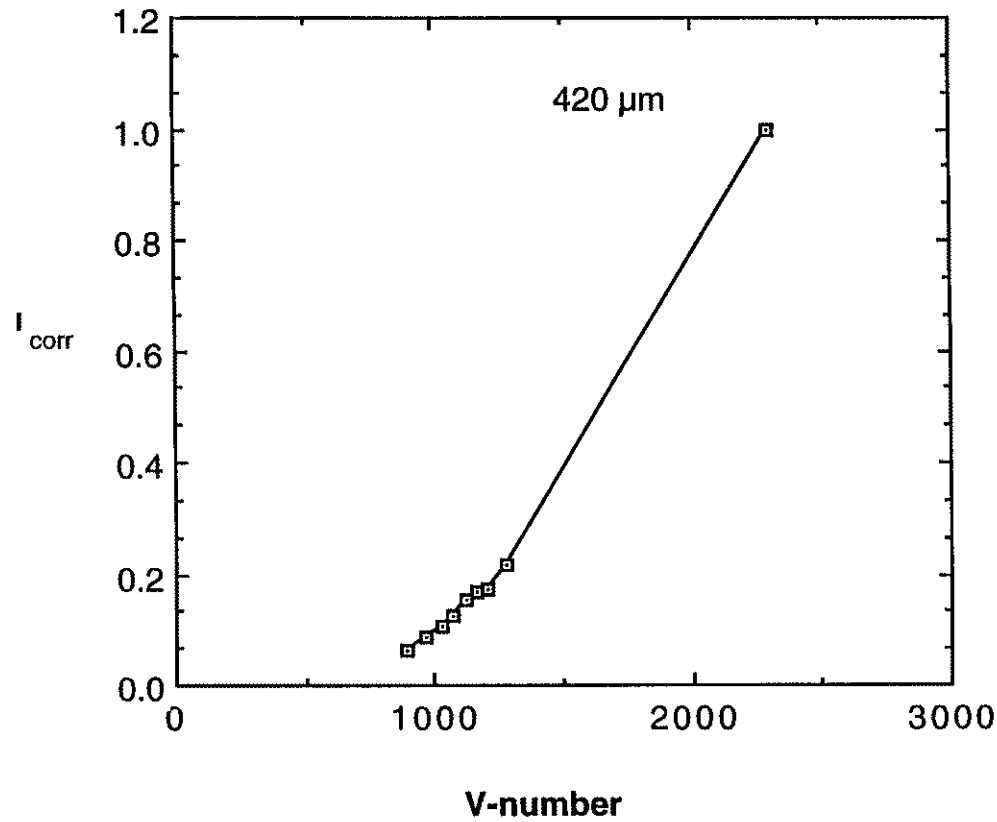

Figure 18. I_{corr} versus V-number for a 420 µm diameter fiber.

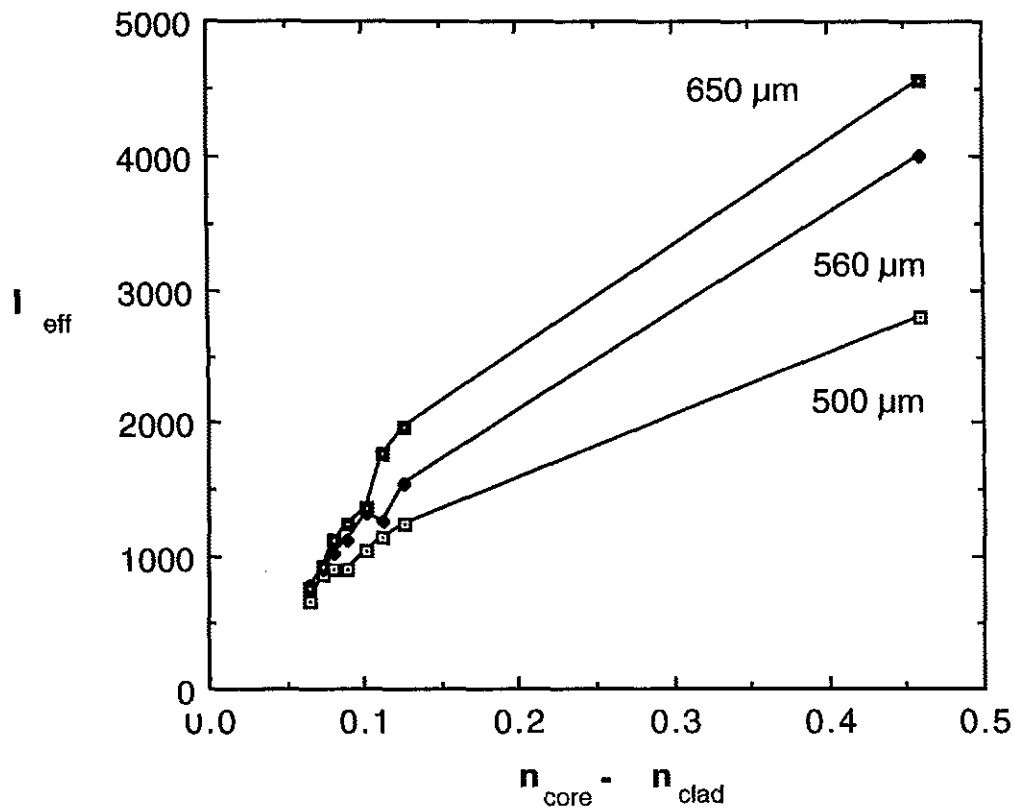

Figure 19. Behavior of intensity,I_{eff}, for fibers of diameters, 500, 560, and 650 µm.

4.4 Normalized Curves

The curves shown in figure 19 were normalized with respect to the highest intensity for each fiber. Figures 20 - 22 show the normalized curves. These graphs better shows the incremental changes in light injection than figure 18. Except for the 500 μm fiber, at larger n_{core}-n_{clad} values the diameter effect is still seen, but at small refractive index differences the incremental changes in intensity are much smaller and the data points are scattered. The scattering and crowding of data points in some instances cause the curves to cross one another at small n_{core}-n_{clad} values. We discuss below some possible sources of the scattering of the data and the difficulties encountered in performing this research.

4.5 Sources of Errors

One major difficulty in performing the experiments in this work was the optical alignment of the cell and the collecting lens. In using a bulk optical lens to collect the fiber emission we were not able to collect all the radiation exiting the fiber. Probably, the most efficient way to collect the emission from the fibers is to use a fiber-optic coupler which attaches to both ends of the fiber and feeds directly to the monochromator. Egalon and Rogowski, and Marcuse [12,13] have indicated that their models were based on the collection of radiation for forward propagating modes only. Thus, equations (2.5) and (2.7) do not take into account the backward propagating modes.

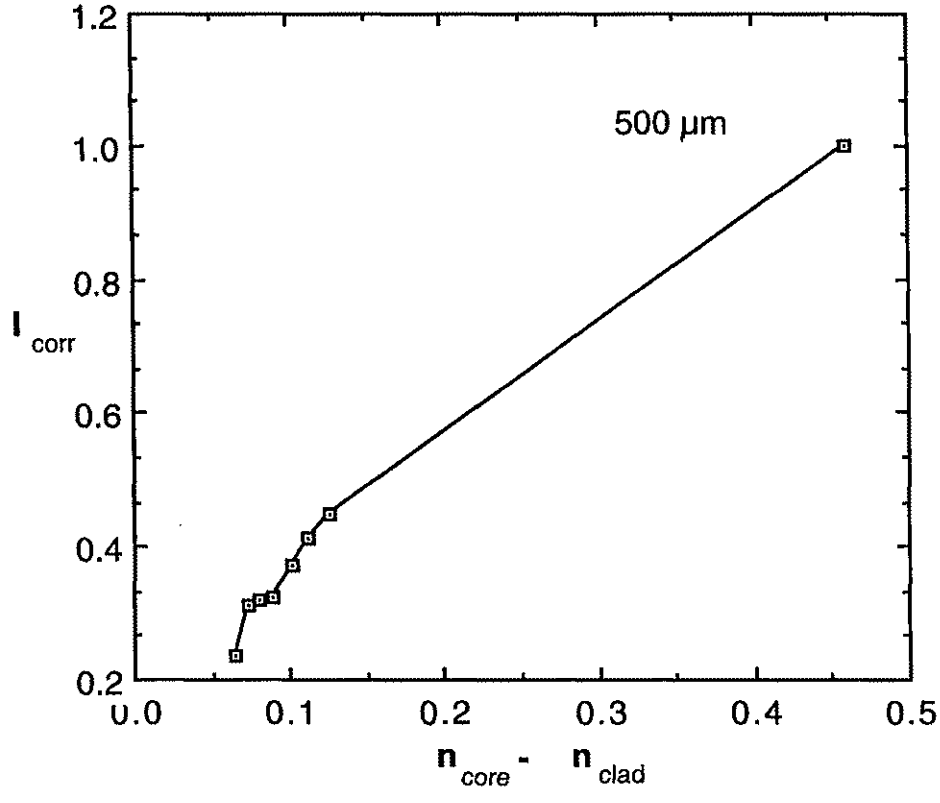

Figure 20. I_{corr} curve for a 500 µm diameter fiber.

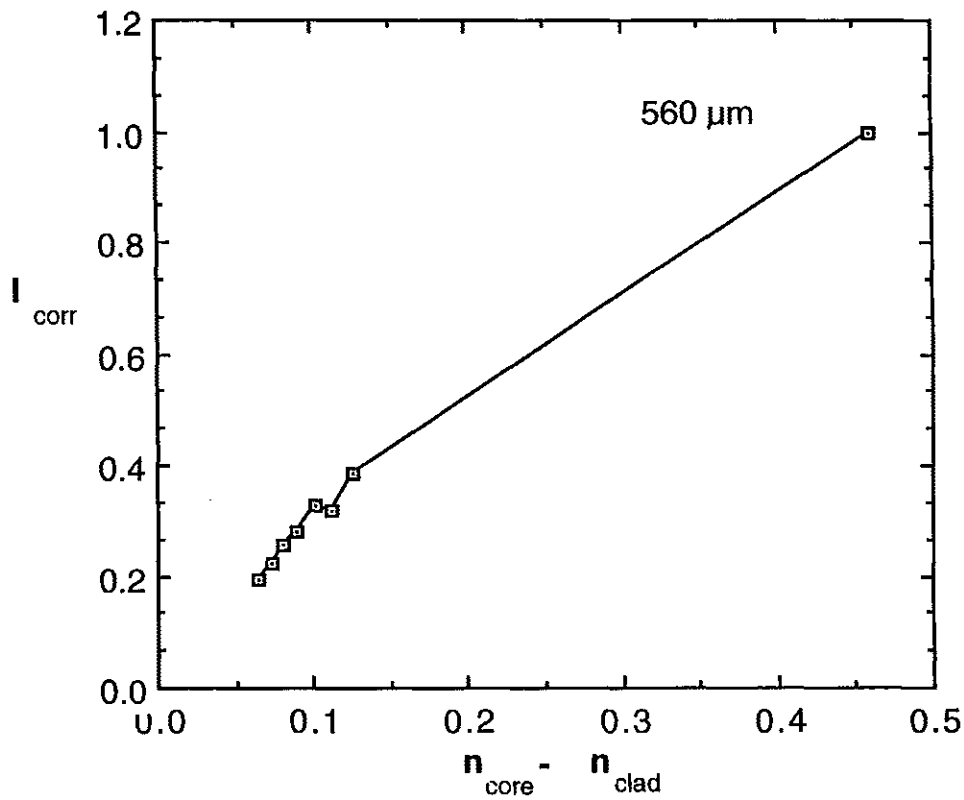

Figure 21. I_{corr} curve for a 560 µm diameter fiber.

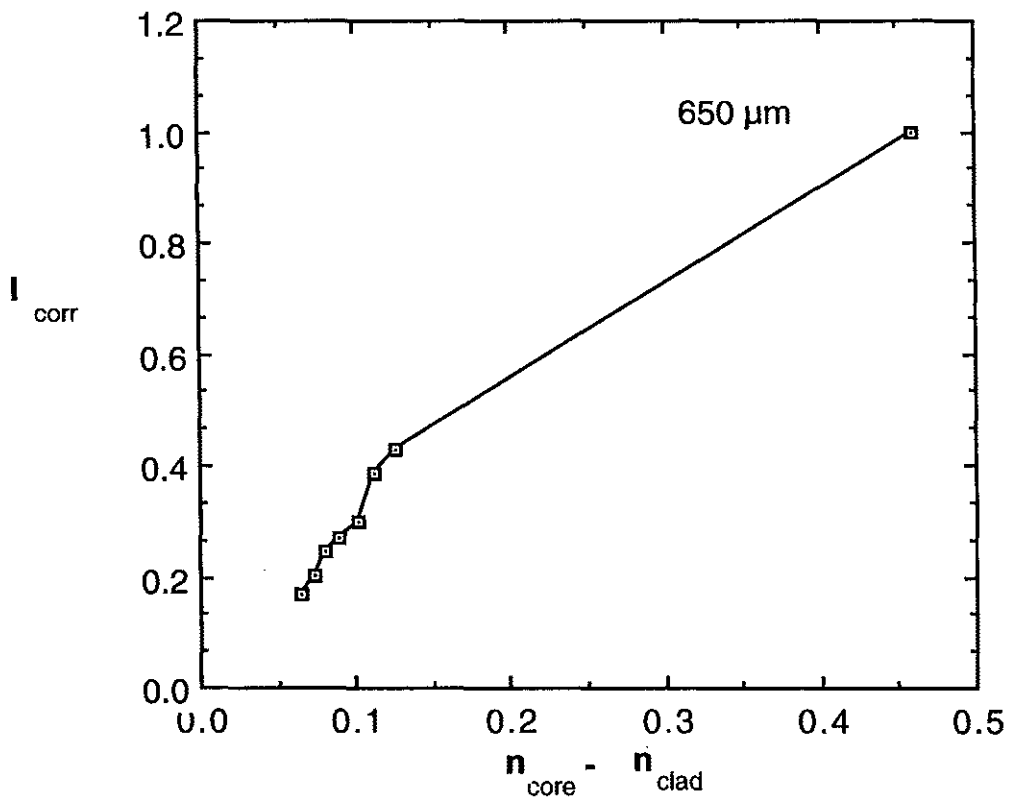

Figure 22. I_{corr} curve for a 650 µm diameter fiber.

Since the signals detected in this work were small in magnitude, background noise was another major problem. Fiber impurities and parasitic emission from the cell wall were the two main sources of noise in the system. The emission from fiber impurities were overcome by side pumping. Initially, we tried exciting the fluorescent sources by axial pumping. While axial pumping did provide the evanescent field needed to excite the sources, it also excited the impurities along the fiber which had emission in the wavelength region of interest. The result was a very low signal to noise ratio, SNR, or a signal that was lost in the noise. With side pumping, we excited only a small fraction of the impurities in the fiber while exciting the entire luminescent region. Side illumination yielded much better results with a minimum SNR of 4:1. To overcome the impurities problem in the future, improved optical quality fiber is required. The other source of noise was light scattered from the cell wall. To reduce this noise, we painted the inside and outside of the plastic tube with flat black paint as previously mentioned in chapter three. Prior to painting the cell, signal detection was almost nonexistent, even for side pumping. Figure 23. shows a typical spectrum from an uncoated fiber. Notice the intensity (counts/sec) is small compared to those of figure 19.

The source of the data scattering for the small n_{core}-n_{clad} value is most probably due to the slight differences in the thickness of the luminescent material. The PDMS coatings were about 10 μm. The theory only address the cases of a bulk (thick) distribution and thin distribution of sources. It does not consider the case where the thin distribution criteria is

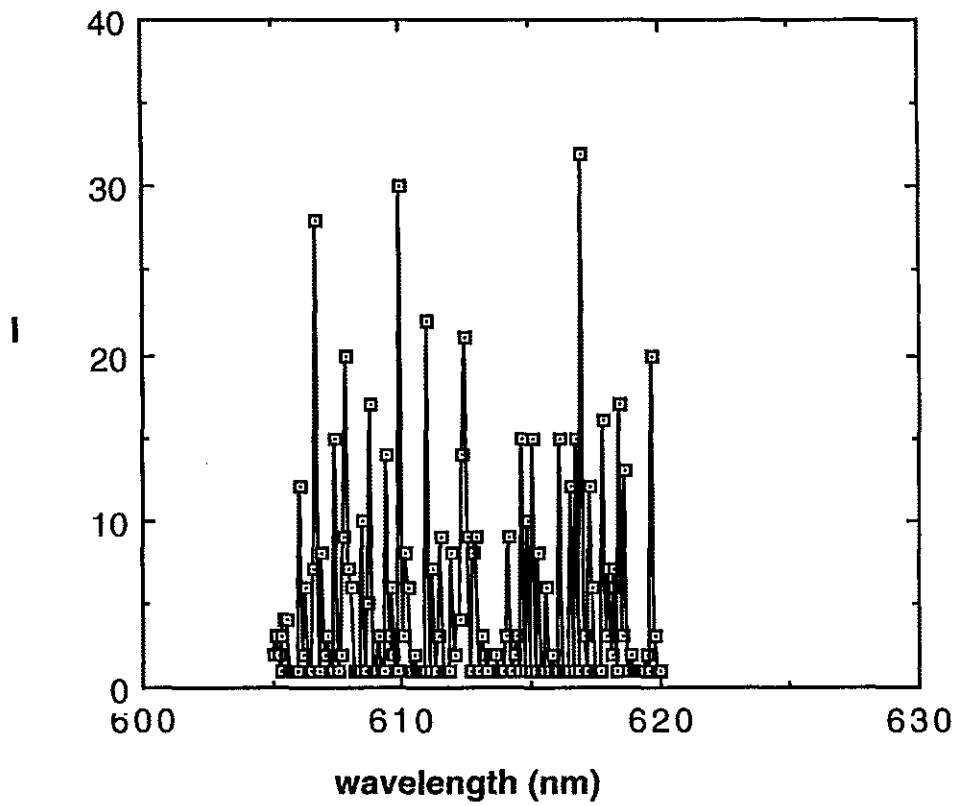

Figure 23. Spectrum from an uncoated fiber.

met but the source thickness is slightly varied. It is our belief that the scattering of the data points at small n_{core}-n_{clad} values is due to slight differences in source thickness. Obviously a fiber with a slightly thicker coating will have a greater volume of sources. Thus, if the 500 μm fiber had a slightly thicker coating than 650 μm fiber, the 500 μm fiber may inject more light into the core at low n_{core}-n_{clad} values because it has more sources emitting. Since there are so many variables involved in the coupling of light into bound modes, it is difficult to know with certainty why the data point are not smooth. At present there is no general theory encompassing all the parameters involve in coupling light from the cladding of a fiber into the core of the fiber. Since a great deal of FOS use standard communication fiber which has a small core-clad refractive index difference, additional theoretical and experimental work is needed to verify that slight changes in thin film distributions are of great concern for these sensors.

CHAPTER 5

CONCLUSIONS AND FUTURE WORK

5.1 Effect of index difference, n_{core}-n_{clad}

The most significant conclusion drawn from this experimental study is that the greater the refractive index difference, n_{core}-n_{clad}, the better the coupling efficiency. This result is in contradiction to the requirements of a standard optical fiber for communication. A standard step index fiber has a very small index difference, n_{core}-n_{clad}. The maximum index difference is obtained for a bare core fiber with air as the clad. As stated earlier, the V-number of a fiber is given as:

$$V = \frac{2\pi a}{\lambda}\sqrt{n_1^2 - n_2^2} \qquad (5.1).$$

The $TE_{0,1}$ and $TM_{0,1}$ modes cut off when $V \leq 2.405$, which is the condition for a single mode operation of a fiber. For a given wavelength, the radius of the single mode fiber can be increased to a maximum when $n_1 \approx n_2$. As an example, for $\lambda = 1\mu m$, the radius of a single mode fiber is 2.21 μm when $n_1 = 1.5$ and $n_2 = 1.49$, and this radius reduces to 0.34 μm when $n_1 = 1.5$ and $n_2 = 1$. For mechanical stability of the fiber, it is better to have a larger diameter which requires a smaller index difference. Another advantage of a smaller index difference is the reduction in mode dispersion.

The signal pulse width broadening due to modal dispersion is given by [21]:

$$\Delta t = \frac{n_1 L}{n_2 c}(n_1 - n_2), \qquad (5.2)$$

where L is the propagation distance and c is the velocity of light in vacuum. For the values of $n_2 = 1$ and 1.49 given above, the pulse width broadening is 2500 and 74.5 nsec/km, respectively. Hence a smaller index difference is preferred. For fluorosensors in which collection of the fluorescent radiation is paramount, our results suggest that standard communication fiber may not be the best choice for the design of optimal sensors. One solution to this problem is to attach (splice) communication fibers to the sensing fiber for simply guiding the signals.

While the power injected into the core increases linearly with the increase in index difference $n_{core}-n_{clad}$, the penetration depth of the evanescent field decreases, as given by (2.3)

$$\delta p = \frac{\lambda}{2\pi\left[n_1^2 \sin^2\theta - n_2^2\right]^{1/2}} . \qquad (5.3)$$

Therefore the volume excited by axial pumping decreases with increase in index difference, which in turn decreases the signal available for coupling into the core. This problem can be overcome by increasing the length of the sensing region.

5.2 Effect of fiber diameter

It is also found that a larger diameter fiber has the ability to collect more cladding fluorescence. Obviously the total number of possible guided modes will increase with the diameter of the fiber; but for small n_{core}-n_{clad} values the increase in injected power is small. This suggest that for good coupling efficiency, a large difference in refractive index between core and cladding, and a moderate large diameter fiber are needed. This will require proper transitions from the ends of sensing fiber to the standard guiding fibers.

5.3 Comparison with theoretical results

As discussed in chapter 2, Marcuse's theory uses the well known weakly guiding approximations to predict the injection efficiency of light from the clad to the core. This is applicable mainly for communication fibers. However, Egalon and Rogowski used exact field solutions for any arbitrary values of refractive indices of the core and clad. Our experimental results are in good agreement with their theoretical predictions that the injection efficiency of cladding sources increases linearly with index difference n_{core}-n_{clad} as presented in chapter 4. However, Love's theory predicts a decrease in injection efficiency with an increase in n_{core}-n_{clad}, which is contrary to our experimental results.

5.4 Applications

A fluorosensor employing the active cladding configuration has a wide range of applications. Any material which produces fluorescence could be used for sensing. Since any changes to the fluorescence properties of the material caused by external perturbations such as temperature, pressure, pH, radiation, can be monitored by using a fluorosensor configuration. Therefore, fluorosensors will found applications in medical, industrial, and environmental systems.
Since the injection efficiency depends on the refractive indices of the core and clad, the experimental setup employed in this study could be used to measure refractive index of an optical fiber. In addition, refractive indices of liquids and solids deposited on a reference fiber could easily be measured.

5.5 Future work

This work employed external excitation to study the injection efficiency. Experiments using axial excitation by the bound modes of the fiber will provide a complementary extension to this work. It is also beneficial to study the differences between sources distributed throughout the bulk of the clad and those at the interface. Also, suitable materials which have refractive index values between 1 and 1.33 are needed to get more range for the data on n_{core}-n_{clad}.

REFERENCES

1. D. Davies and S. Kingsley, Electron. Lett. 10, 21 (1974)

2. H. Arditty, J. Dakin, and R. Kersten (eds.), "Optical Fiber Sensors," Springer-Verlag: Berlin, (1989).

3. E. Udd (ed.), "Fiber Optic Sensors," Wiley-Interscience: New York, (1991).

4. W. Philp, D. Booth, A. Shelamoff, and M. Linthwaite, Meas. Sci. Technol. 3, 603, (1992).

5. R. Kopelman, W. Tan, and Z. Shi, SPIE Proc., 1796, 157, (1992).

6. S. Syracuse, D. Ferrell, E. Schmidlin, E. Mendoza, A. Khalil, and R. Lieberman, SPIE Proc., 1796, 178, (1992).

7. P. Cielo, J. Krapez, and M. Lamontagne, Opt. Eng., 32, 486, (1993).

8. G. L. Mitchell, in "Fiber Optic Sensors" E. Udd (ed.), Wiley, New York, p.140, (1991).

9. R. A. Leiberman, L. Blyer and L. Cohen, IEEE J. Lightwave Technol. 8, 212 (1990).

10. S. Albin, "A Distributed Fiber Optic Radiation Sensor," U.S. Patent (Pending).

11. W.F. Love, L. J. Button, and R.E. Slovacek, "Optical Characteristics of Fiberoptic Evanescent Wave Sensors" in "Biosensors with Fiberoptics," Wise and Wingard (eds.), The Humana Press, (1991).

12. D. Marcuse, "Launching Light into Fiber Cores from Sources Located in the Cladding," IEEE J. Lightwave Technol. 6, 1273, (1988).

13. C.O. Egalon and R. S. Rogowski, Theoretical model for a thin cylindrical film optical fiber fluorosensor, Opt. Eng., 31, 237, (1992).

14. C. O. Egalon, "Injection Efficiency of Bound Modes," Ph.D thesis, The College of William and Mary, Williamsburg, VA., (1990).

15. P. Yeh, "Optical Waves in Layered Media," Wiley-Interscience: New York, p. 70, (1988).

16. "CRC Handbook of Chemistry and Physics, 59th edition, R. Weast and M. Astle (eds.), E-358, (1978).

17. K. Wickersheim and R. Lefever, J. Electrochem. Soc.,111, 47, (1964).

18. N. Chang, J. Appl. Phys., 34, 3500, (1963).

19. F. Pedrotti and L. Pedrotti, "Introduction to Optics," Prenctice-Hall: New Jersey, p. 476, (1987).

20. S. Albin, A. Bryant, C. Egalon, R. Rogowski,and J.Nankung, "Experimental Verification of a Theoretical Model of an Active Cladding Optical Fiber Fluorosensor"Chemical, Biochemical, and Environmental Sensors IV, SPIE Proc.,1796, 393, (1992).

21. K. Jones., "Introduction to Optical Electronics," Harper & Row: Cambridge, p.53, (1987).

APPENDIX

PUBLICATIONS FROM THIS STUDY

1. S. Albin, A. Bryant, C. Egalon, R. Rogowski, and J.Nankung, "Experimental Verification of a Theoretical Model of an Active Cladding Optical Fiber Fluorosensor"Chemical, Biochemical, and Environmental Sensors IV, SPIE Proc.,1796, 393, (1992).

2. S. Albin, A. Bryant, C. Egalon, R. Rogowski, and J.Nankung, "Injection efficiency from a side excited thin film fluorescent cladding of a circular waveguide" Accepted July 93 for Publication in Opt. Eng.

3. A. Bryant, S. Albin C. Egalon, and R. Rogowski, "Effect of Numerical Aperture on the Injection Efficiency of a Fluorosensor" To be presented at the Electro Optics Conference, Hampton University, September, 22-23, 1993.